



Acoustics 2019

Sound Decisions: Moving forward with Acoustics

Prediction of small-scale rotor noise using a low-fidelity model-based framework

Li Chen (1), Trevor Batty (2) Matteo Giacobello (2) and Ronny Widjaja (2)

(1) Maritime Division, Defence Science and Technology Group, 506 Lorimer Street, VIC 3207, Australia
(2) Aerospace Division, Defence Science and Technology Group, 506 Lorimer Street, VIC 3207, Australia

ABSTRACT

A model framework for rapid assessment of the noise generated by small-scale rotors, such as those found on small Uninhabited Aerial Systems (sUAS), is presented. The acoustic signatures of two commercially available 2-blade rotors in hover conditions are considered, namely the DJI-CF 9.4x4.3 and APC-SF 11x4.7 which have a diameters 0.24 m and 0.28 m, respectively. The model framework is based mainly on semi-empirical models with limited inputs from Computational Fluid Dynamics (CFD) based solutions. Supplementing the models using CFD-based solution inputs leads to a improved acoustic signature prediction. The predicted noises of both narrow-band and broadband are compared with the experimental measurements, and the agreement is found to be reasonable.

1 INTRODUCTION

Over the last decade there has been a marked increase in the use of small Uninhabited Aerial Systems (sUAS) to fulfil a range of different missions, such as target detection and surveillance. In order to conduct these missions, it is often necessary for the UASs to work in close range to the target, and therefore their detectability and tractability become important metrics in their performance and overall mission success. According to Berardini et al (2017), an effective approach to detect a sUAS is to measure its acoustic signature and therefore being able to predict the acoustic signature crucial to manage its detectability. In a commercial and recreational context, the use of UASs in an urban environment has seen increase regulation. Although this does not currently cover acoustic emissions, growing public concern is expected to see sUAS noise classification and restrictions in the near future. While the main focus of sUAS design optimisation have been devoted to their performance and efficiency (Deters and Selig 2008, OI et.al. 2008), the acoustic signature of those systems has attracted relatively less attention to date (Tinny and Sirohi 2018, Zawodny et al. 2018).

The acoustic signature of sUAS is the product of source generation and radiation. Although some noise sources are weak in nature, an effective radiation mechanism can still result in strong acoustic levels. For example low-Mach-number-flow-induced noise from rotors or propellers, can produce a strong acoustic signature and compromise their clandestine operation. A good overall acoustic signature management strategy should include due consideration to the rotor or propeller noise generation and its mitigation, which in turn requires a thorough understanding of the underlying physics, such as source generation mechanisms and sound radiation characteristics, as well as accurate prediction methods. There are a number of well accepted models for the aeroacoustics of full-scale helicopters, but due to the Mach number and Reynolds number disparity, their applicability to small scale sUAS has not yet been fully assessed (Zawodny 2018). In this paper, a framework mainly based on low-fidelity analytical and semi-empirical models for predicting the acoustic signature of sUAS is presented. The model framework is applied to the commercially available 2-blade rotors, the DJI-CF and APC, for assessing the tonal and broadband component of their acoustic signature in hover conditions. The predicted sound levels are compared with the experimental measurements of Zawodny et al. (2018).

2 MAIN NOISE SOURCES OF A SMALL UAS

Sound radiated from a sUAS rotor can be classified into narrow-band (tonal/deterministic) and broadband components. The narrowband noise sources can be further divided into steady and unsteady loading noise and thickness noise. According to Brooks et al.(1989) and Blake (1986), the rotor broadband noise contributions comprise: (i) leading-edge (LE) noise, including turbulence ingestion noise and blade-wake interaction noise; (ii) turbulence boundary layer trailing-edge (TE) noise; (iii) blunt trailing-edge vortex shedding noise; (iv) tip-vortex noise; (v) laminar boundary layer transition noise and (vi) flow separation at large angle-of-attack noise. Blunt TE noise is associated with the interaction of the vortex shedding and the TE. Tip vortex noise can be considered as part of TE noise because it arises by the interaction between the vortex structure and the passing trailing-edge.

The steady loading noise of the rotor is generated by a rotational dipole, thus is narrow-banded and of a typical dipole directivity. The loading on the rotor is steady in the rotating frame but unsteady in the stationary acoustic medium and generates tonal noise at the harmonics of blade-passage frequency (BPF). This noise source becomes significant for high Mach number flows. At low rotor tip speed (low Mach number flow), this noise is normally low compared to other noise sources except for the thickness noise contribution. The steady noise is related to the lift force and its distribution on the rotor blade. The thickness noise is generated by the acceleration of flow local to the rotor as the blade passes through. Like the steady noise, the fluid expansion about the blade profile is steady in the rotating frame but unsteady in the acoustic medium. This noise source is monopole-like but has dipole directivity due to the Doppler amplification and becomes significant only when the tip speed is high (high Mach number flow). For low tip speed, this noise is lower than steady loading noise. In this paper, only steady loading noise is relevant and analysed.

The LE noise is generated by the interaction between turbulence and the LE of rotor blades, leading to strong force fluctuations and generation of a high dipole sound. This noise source can produce both tonal and broadband noise depending on the characteristics of the turbulent flow that the blades encounter. Another important contribution to the broadband noise source is TE noise, which is generated by turbulent flow passing the TE of rotor blades. The TE efficiently scatters the turbulence into radiated noise. This noise is broadband in nature and well accepted as being an important noise source for low Mach number flows. Other broadband noise, such as TE bluntness and tip-vortex noise are generated by the interaction between the vortex shedding and the TE.

3 MODEL FRAMEWORK

The governing equation for sound pressure radiation from turbulent flows can be written as

$$\frac{\partial^2 p}{\partial t^2} - c_0^2 \nabla^2 p = \frac{\partial}{\partial t} [Q\delta(f)] - \frac{\partial}{\partial x_i} [F_i\delta(f)] + \frac{\partial^2}{\partial x_i \partial x_j} [T_{ij}H(f)] \quad (1)$$

The terms on the right hand side of Eq. 1 are monopole, dipole and quadrupole noise sources, respectively. Here Q is the rate of mass injection per unit volume, F_i is the component of force vector per unit volume normal to i , and T_{ij} is the stress tensor. The loading and LE noises attribute to the dipole source, and thickness noise source is monopole. The TE noise attributed to the quadrupole source. Different sources listed in the previous section are modelled by either an analytic or a semi-empirical model. The noise prediction process is outlined in the model framework shown in Figure 1.

The tonal noise are predicted using Hanson's analytic solutions (1980), and the model of Blake (1986) is also tested. The broadband noises, except the LE noise, are predicted using both BPM model of Brooks et al. (1989) and the model of Chen & McGillivray (2014). The LE noise is predicted using the model of Amiet (1978). The inputs for those models are the aerodynamic conditions experienced by the rotor blades, which are obtained either from CFD simulations or simplified aerodynamic models.

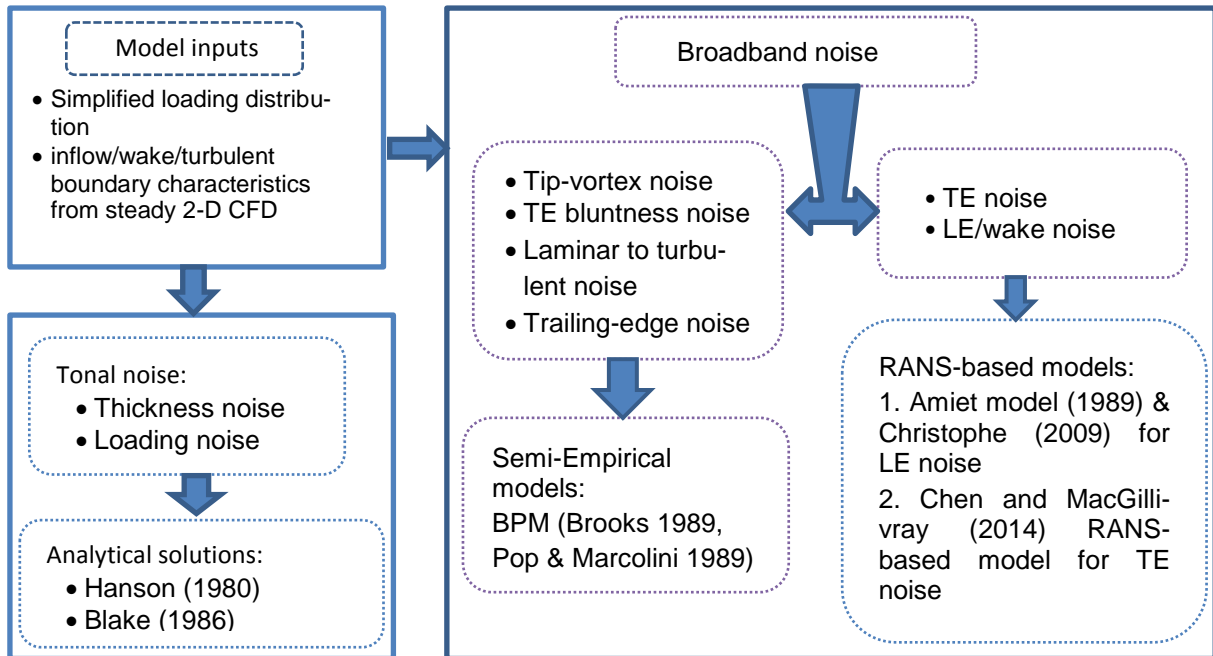


Figure 1 Model framework

3.1 Bench-mark rotor blades

Two commercial available rotors, DJI-CF and APC-SF, are used to assess the accuracy of the model framework. The nominal geometric properties of two rotors is obtained from the work of Zawodny et al. (2018), and the schematics of the rotors are shown in Figure 2. The DJI-CF rotor has a diameter of 24 cm while the APC-SF propeller is of diameter 28 cm. These blades we also laser scanned for the purpose of generating CAD surfaces from which a 2-D structured mesh could be generated for input into the CFD analysis. It should be noted that there was some differences found between the nominal geometric data from Zawodny et al. and the scanned geometry, which may be attributed to manufacturing variation. The measured pitch angles from the scan were 7.63° and 10.20° at $0.75R$, where R is the rotor radius, for the DJI-CF and APC-SF rotors respectively. Hence these pitch angles were used in the CFD analysis, rather than the nominal published values of 8.36° and 9.20° respectively.



Figure 2 Benchmark 2 blade rotors

4 RESULTS

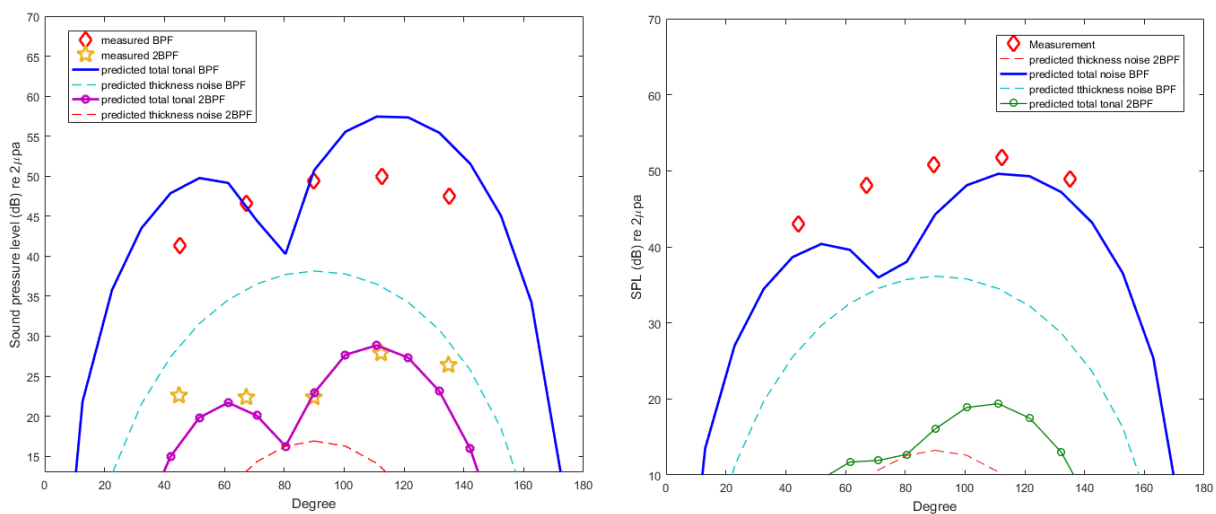
The acoustic signatures of two rotors in a hover condition were predicted for standard sea level conditions and operation condition of 5400 RPM for the for DJI-CF and 4200PRM for the APC-SF rotor. The corresponding Reynolds numbers for DJI-CF and APC-SF are 5.14×10^4 and 9.00×10^4 respectively.

4.1 Tonal noise

The total tonal noise arising from the steady loading noise and thickness noise is predicted using the model of Hanson (1980). The predicted results are compared with the measured data of Zawodny (2018). As a further comparison, the steady loading noise model of Blake (1986) is also tested. The inputs, such as the rotor thrust and geometric information required by the model are obtained from Zawodny (2018). It should be noted that the loading distributions along both the chordwise and spanwise directions are simplified in the calculation. For the chordwise direction, the loading distribution is assumed to be uniform, while for the spanwise direction, a piecewise linear distribution is assumed. However, it is possible to implement other more accurate loading distributions, such as from a 3D CFD analysis, which should lead to more accurate estimation of the tonal noise. This will be considered in a follow-on study.

The comparison between the predicted and experimentally derived sound pressure level (SPL) and directivity at two blade passing frequencies (BPF) are shown in Figure 3. Here the the angle 90° is aligned with rotor disc plane and 0° and 180° degrees coincide with the upstream inflow into the rotor and downstream outflow, respectively. Figure 3(a) shows the results DJI-CF rotor at 5400RPM and Figure 3(b) is for APC-SF rotor at 4200RPM. It can be seen that for both rotors the steady loading noise dominate the tonal noise at two BPFs, and the thickness noise is low in each case. The predicted total tonal noise for DJI-CF at the second BPF agrees better with the measurements in terms of the directivity and magnitude. The predicted tonal noise levels at the first BPF for DJI-CF rotor agree well at the angles between 60° - 100° , and the predicted tonal noise level at the first BPF for APC-SF agree well at the angles outside of that range. It has been found that the noise is decreasing significantly at BPF higher than 2BPF.

The performance of Blake's model for the loading noise is examined, and the results are given in Figure 4. It can be seen that the loading noise predicted by Blake's model is 25 dB higher than that using Hanson's model, however the two models give a similar directivity.



(a) DJI-CF at 5400RPM

(b) APC-SF at 4200RPM

Figure 3 SPL comparison of the predicted tonal noises and its directivity with measured data

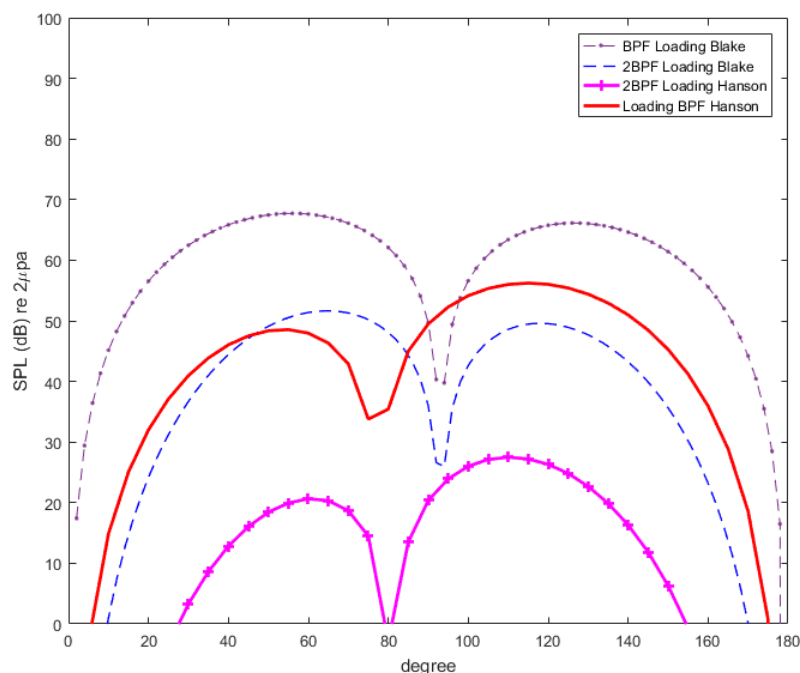


Figure 4 SPL comparison between different models for tonal noise (DJI-CF at 5400 RPM)

4.2 Broadband noise

As noted in model frame work presented in Figure 1, the prediction of the broadband noise used CFD-based simulations to enhance the prediction capability of the empirical models. A brief description of the CFD approach is introduced in the following section, before presenting comparisons of predicted and experimentally measured noise spectrums.

4.2.1 CFD simulation of 2D flow over single blade of DJI-CF and APC-SF rotor

The 3D geometry of each of the blades were obtained via a laser scanning metrology process. A cross-section of each blade at 0.75R was taken and a smooth curve lofted through the points. An induced inflow angle-of-attack was calculated using the approximation from Chen (1989). This required a lift curve slope, which was calculated by running an angle-of-attack sweep using the XFOIL software package version 6.96 from Drela (1989). By forcing transition to turbulent flow in XFOIL at 5% of chord, the lift curve slopes in the linear pre-stall region were obtained as 5.439 rad^{-1} and 6.146 rad^{-1} for the APC and DJI cross-sections at 0.75R respectively. This resulted in calculated effective angles-of-attack, defined as the blade pitch minus the induced inflow angle, of 4.63° and 3.59° for the APC and DJI profiles, respectively. It should be noted that the physical APC blade, along with the scanned geometry, had a fine burr on the leading and trailing edges, associated with the injection molding manufacturing process. These were retained in the surface model used as the basis for the CFD analysis.

For each blade profile, a 2D structure mesh with a C-topology was then generated using Pointwise V18.2 R2. In each case the profile pitch was set at the appropriate effective angle-of-attack. Care was taken to ensure the first wall-normal cell height on the blade was approximately $y^+ = 1$ to ensure a resolve-to-the wall Reynolds-Average Navier-Stokes solution. The far-field boundary was approximately 75 chord lengths and centred on leading edge of the blade. A mesh resolution and domain size sensitivity was also performed to verify the suitability of these parameters.

ANSYS Fluent 19.2.0 was used as the CFD solver and the $k-\omega$ turbulence model with the Shear Stress Transport (SST) formulation being enabled. The temperature and density at standard sea-level conditions was set, at 288.15 K and 1.225 kg/m^3 respectively.

Solutions for the DJI profiles showed good numerical convergence, with the residuals dropping several orders of magnitude and force monitors reaching steady values. The APC blade did not converge to a steady solution, as

the lip at the sharp LE caused the flow to detach and then reattach shortly downstream. The lip on the trailing edge caused eddies to shed from the trailing edge in pairs, first from the top surface, then from the bottom surface.

The resultant profiles of mean turbulence dissipation rate, mean turbulence intensity field and mean turbulence kinetic energy field, at a distance downstream of the blade which corresponded to the inflow to the next blade were extracted. As the APC solution was of oscillatory nature, the profiles were averaged over a series of oscillatory cycles.

4.2.2 Noise prediction

The BPM model of Brooks et al. (1989) has been used to estimate the TE noise, the tip-vortex noise, the blunt trailing-edge vortex shedding noise and laminar flow-to-turbulent transition noises.

The LE noise is generated from the turbulence impingement on the LE of rotor blade, and this turbulent inflow of the rotor blade is the wake of the upstream rotor blade which is obtained by the steady CFD solution. The 2D CFD simulations are conducted at the local resultant velocity at $0.75R$ and turbulence quantities in the wake, such as turbulent kinetic energy and dissipation rate are used to estimate the turbulent spectrum near the LE. The downstream distance at which the wake was sampled corresponds to the circumferential distance between the blades, that is $\pi(0.75R)$, to represent the injection of the upstream blade wake on the trailing blade.

In the calculation of the LE noise, it is assumed that the streamwise turbulent length-scale is constant over the span of the rotor blade, and the variation of the turbulent spectrum along the span is purely due to the change of the resultant velocity. The rotor blade is divided into 40 strips along the span, and the total LE noise is the summation of noise from each of 40 elements using the method presented by Christophe & Anthoine (2009). The comparison of using Amiet model combined with the method of Christophe & Anthoine (2009) and with a uniform blade of a representative velocity at $0.75R$ is shown in Figure 5. The results which use the Amiet model combined with the Christophe & Anthoine is referred to as the “total noise strips” and with the uniform blade of a representative velocity at $0.75R$ as “total noise $0.75R$ ”. It can be seen that for both rotors the results obtained by assuming a blade with a constant chord (based on the $0.75R$ location) are slightly higher than the inverse method of Christophe & Anthoine (2009).

The contributions of different noise sources to the total broadband noise for DJI-CF rotor are shown in Figure 6. It can be seen that the vortex shedding noise is a major contributor to the total noise at the frequency of 16 KHz, but the LE noise is the dominant broadband noise source across almost all other frequencies. The predicted TE noise is much lower. The tip-vortex interaction noise and the laminar-to-turbulent flow transition noise are very low and are not shown here.

The comparisons between the predicted and measured broadband noise for the two rotors at two observation points of 45° and 22.5° are shown in Figure 5. For the DJI-CF rotor, the LE noise dominates the broadband noise (Figure 5a). However, for APC-SF rotor, no dominant vortex shedding noise was measured or predicted (Figure 5b). Similar to DJI-CF rotor, for APC-SF rotor, the leading-edge noise dominates the broadband noise at the frequency higher than 1 KHz. The predicted total broadband noise levels show a reasonable agreement with the measurements for that frequency band, particular at the observation point of 22.5° . For DJI-CF rotor, the predicted sound levels match well at frequencies higher than 4 kHz. However, the predicted sound levels show a poor correlation with the measurements at the frequencies lower than 3 KHz for DJI-CF rotor and 1 KHz for APC-SF rotor. In order to investigate the cause of those discrepancies, the displacement turbulent boundary thickness required by BMP model was extracted directly from the CFD solution instead of using the approximation, however no improvement was obtained.

A further investigation of the cause was to apply the CFD-RANS-based trailing-edge noise model of Chen & MacGillivray (2014) to the DJI-CF rotor, and the predicted results are included in Figure 5(a). It can be seen that the total broadband noise predicted using the RANS-based model has shown a much better agreement with the measurement at the frequencies lower than 5 KHz. The peak of trailing-edge noise is at 1.6 KHz. The broadband noise at the frequencies lower than 5 KHz is mainly due to the TE noise. It should be noted that the CFD solution is a 2D simulation at Reynolds number based on a spanwise location of $0.75R$, thus an overestimation would be expected due to neglecting the variation of Reynolds numbers along the rotor span.

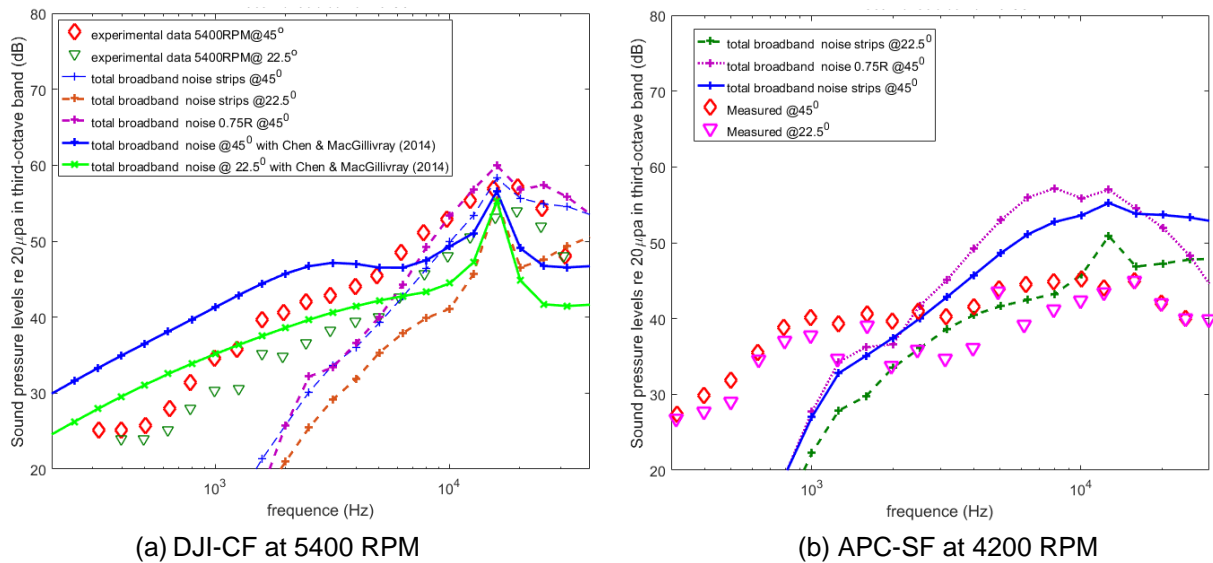


Figure 5 SPL comparison between that measured by Zawodny et. al (2018) and the predicted broadband noise for DJI-CF at 5400 RPM

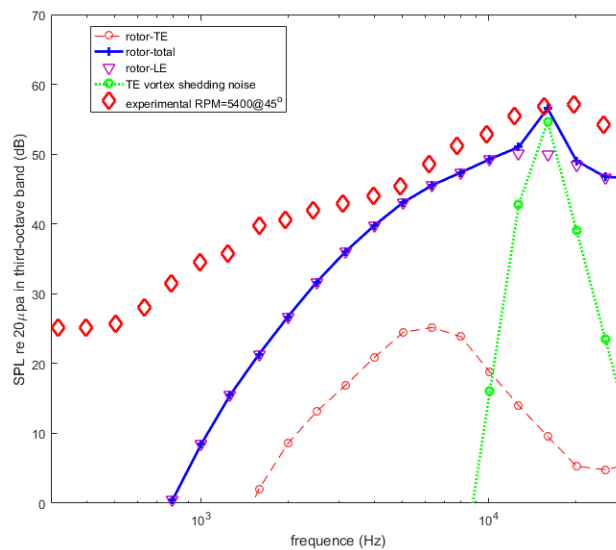


Figure 6 SPL contributions of different noise sources to the total broadband noise for DJI-CF at 5400RPM

CONCLUSIONS

A model framework based mainly on the low-fidelity semi-empirical models for small scale rotor noise is presented. The aerodynamic noise produced by two rotors, DJI-CF operating at 5400RPM and APC-SF at 4200RPM is estimated using the framework. The predicted tonal and broadband noises are compared against the experimental measurements, and the agreement is found to be reasonable. For tonal noise, the prediction can be improved with more accurate properties of the rotor blade such as the rotor cross-section geometry and loading distribution. For broadband noise, it has been found that the leading-edge and trailing-edge noise are major noise sources. Its is expected that the prediction can be improved by using the CFD-RANS based model inputs in the framework. A more accurate prediction of the broadband noise can be achieved with a full 3D CFD simulation that will provide a more accurate flow around the rotors and the inputs required by the leading-edge noise and trailing-edge noise models.

REFERENCES

- Deters, R.W., Selig, M.S. 2008, 'Static testing of micro propellers', *26th AIAA applied aerodynamics conference*, AIAA paper 2008-6246, Aug.
- Ol, M., Zeune, C., Logan, M. 2008, 'Analytical-experimental comparison for small electric unmanned air vehicles', *26th AIAA applied aerodynamics conference*, AIAA paper 2008-7345, Aug.
- Tinney, C.E. and Sirohi, J. 2018, 'Multirotor drone noise at static thrust', *AIAA Journal*, 56 (7), pp. 2816-2816.
- Zawodny, NS, Boyd Tr., DD and Burley CL, 2018, 'Acoustic characterization and prediction of representative small-scaled rotary-wing unmanned aircraft system components', NASA report 20160009054.
- Brooks, TF, Pop DS and Marcolini MA, 1989, 'Aerofoil self-noise and prediction', NASA RP 1218.
- Chen, L. and MacGillivray, I., "", *AIAA Journal*, Vol. 52(14) pp. 2673-2681, 2014.
- Blake, W, *Mechanics of Flow-induced sound and vibration Vol II*, ACADEMIC PRESS. INC, ISBN 0-12-103502-6.
- Drela, M., 1989, 'An Analysis and Design System for Low Reynolds Number Airfoils', Conference on Low Reynolds Number Aerodynamics, University of Notre Dame, Notre Dame, Indiana, June 1989
- Hanson, D.B, 1980, 'Helicoidal surface theory for harmonic noise of propellers in the far field', *AIAA* **18**(10), 1213-1220.
- Chen, R.T.N, 1989, 'A Survey of Nonuniform Inflow Models for Rotorcraft Flight Dynamics & Control Applications'.
- Amiet R.K., 1975, 'Acoustic radiation from an aerofoil in a turbulent stream', *J. Sound & Vibration*, 41(4), 407-420.
- Christophe, J. and Anthoine, J., 2009, "Amiet's theory in spanwise-varying flow conditions", Technical Note, *AIAA Journal*, 47(3), 788-790.